Metabolically Driven Differentiation of Human Pluripotent Stem Cells to Generate Robust and Functional Lymphatic Endothelial Cells

Donghyun Paul Jeong[1,2], Sanjoy Saha[1,3], Daniel Montes-Pinzon[1,2], Angela Taglione[3], N. Keilany Lightsey[1,3], Rananjaya Subash Gamage[1,3], Brendan Stein[1,2], James Brandon Dixon[4], Donny Hanjaya-Putra[1,2,3,5]

[1]Bioengineering Graduate Program, University of Notre Dame, Notre Dame, IN 46556

[2] Aerospace and Mechanical Engineering, University of Notre Dame, Notre Dame, IN 46556

[3] Chemical and Biomolecular Engineering, University of Notre Dame, Notre Dame, IN 46556

[4]The George W. Woodruff School of Mechanical Engineering, Georgia Institute of Technology, GA 30332

[5]Center for Stem Cell and Regenerative Medicine, University of Notre Dame, Notre Dame, IN 46556

Address correspondence to:

Donny Hanjaya-Putra

2010G McCourtney Hall East

University of Notre Dame

Notre Dame, IN 46556

Email: dputra1@nd.edu

Phone: 574-631-2291

Abstract

The lymphatic system plays various crucial but underappreciated roles in fluid transport and immune response in numerous organs and tissue types. Consequently, generation of lymphatic vessels has been postulated as an innovative therapeutic strategy for various diseases. However, there is a lack of efficient and reliable method to differentiate human pluripotent stem cells into lymphatic endothelial cells (LEC) for lymphatic regeneration. Current differentiation methods suffer from poor yield and low lymphatic marker expression, while also having limited clinical applicability due to its reliance on either the embryoid body intermediates or xenogenic supporting cells. Here, we develop a stepwise differentiation method that relies on fully defined treatment with sodium acetate, a metabolite resulting from fatty acid oxidation, along with VEGF-C, that yields high expression of lymphatic marker and retain the functionality of native LECs. We show that differentiated LECs (dLEC) express comparable levels of lymphatic markers compared to native LECs, which is up to 15 times higher than the current leading standard of dLECs. We also show that the dLECs can form lymphatic vascular networks in 2D and 3D and secrete important lymphangiocrine for organ maturation. Upon implantation into murine lymphedema models, dLECs were able to integrate with the host lymphatic vessels, restore fluid flow, and reduce swelling. In conclusion, our functional dLECs can be incorporated into novel tissue engineering applications in personalized therapies and disease modeling, as well as provide a direct therapeutic option for lymphedema and lymphatic disorders.

Introduction

The lymphatic system is a secondary circulatory system that works in conjunction with the blood vessels to maintain fluid homeostasis, lipid transport, and immune trafficking.[1–3] The lymphatic system consists of lymph nodes, lymphoid organs, and lymphatic capillary vessels and ducts, which collect the fluid coming from capillary filtration from the blood vessels and return them back into circulation.[4,5] Despite their importance, the lymphatic system is not as well-understood compared to its blood counterpart, in part due to a relatively small list of lymphatic markers that distinguish it from the blood circulatory system.[6] In a circulatory system including the lymphatics, endothelial cells (ECs) constitute the inner lining of vessels and therefore serve as the direct barrier between the fluid, either blood or lymph, and the tissue.[7] Therefore, ECs play a key role in regulating vessel permeability, constriction, and flow rate, and at times even plays an endocrinal role by producing cytokines that are important for organ maintenance and maturation.[8–11] Likewise, lymphatic endothelial cells (LECs) play a similarly important role in regulating lymphatic performance. Proper network formation of LECs is important for preventing swelling that is commonly associated with lymphatic diseases such as lymphedema.[12,13] LECs also secrete lymphangiocrines such as reelin which play a role in cardiac tissue maturation and other organ development.[14,15]

Because of their importance, LECs derived from human induced pluripotent stem cells (hiPSCs) have been a focus of research in the field of lymphatics. These human differentiated (dLECs) have therapeutic potential as they can promote lymphangiogenesis for wound healing and lymphatic remodeling for lymphedema patients.[16,17] They are also crucial for developing hiPSCs-derived engineered tissues that are physiologically relevant and for studying the interaction between lymphatic system and tumor cells.[18,19] However, existing studies on hiPSCs-derived endothelial cells have mostly focused on blood vasculature system, mainly due

to the difficulty of specifically targeting LECs which are similar to ECs in biomolecular and physiological characteristics. Existing differentiation protocols mostly rely on the formation of embryoid body intermediates or xenogenic supporting cells (i.e., mouse stromal cells, OP9), which suffer from low differentiation efficiency, reduced viability, and low clinical applicability due to xenogenic cells.[20–22]

Further complicating the efforts to develop hiPSCs derived dLECs is the lack of definitive theory on the origin of LECs during embryonic development. The centrifugal theory posits that the lymphatic vessels develop by sprouting from venous endothelium, whereas the centripetal theory suggests that the lymphatic vessels are formed from the mesenchymal cells undergoing *in situ* differentiation.[23] Human iPSCs, given their analogous nature to embryonic cells, can be differentiated to target mature cells by mimicking the embryogenic environments associated with the target cell line.[24–26] Therefore, it is intuitive that differentiation of hiPSCs to LECs should also follow the embryogenic origins of LECs. There have been some evidence that transdifferentiation from BECs to LECs is possible, and other papers have identified pathways that regulate the LEC-BEC separation.[27,28] However, a recent study into EC specification during mouse embryogenesis discovered that Prox1 and LYVE-1 positive LECs are derived from angioblasts rather than venous ECs, suggesting that a viable pathway of LECs differentiation directly from hiPSCs through angioblast stage is possible.[29]

n this study, we focus on unique metabolic characteristics of LECs to further push the differentiating ECs to lymphatic phenotype. Previous approaches have relied mainly on LEC-specific growth factors such as vascular endothelial growth factor-C (VEGF-C), which is a ligand to LEC-specific vascular endothelial growth factor receptor-3 (VEGFR3).[20,30,31] In addition to growth factors, we focus on the LEC's unique dependence on fatty acid metabolism for its energy needs and gene expression. Native LECs are exposed to highly hypoxic environment of the lymph, which force LECs to rely more on anaerobic metabolism.[32] In

addition, fatty acid oxidation (FAO) produces acetyl-CoA, which is used for histone acetylation of VEGFR3, a lymphatic marker that has a positive feedback loop with Prox1, the master lymphatic regulator gene.[33,34] Therefore, we explore the use of FAO-related metabolites in addition to growth factors to efficiently differentiate hiPSCs to LECs. Here, we propose a growth factor and metabolite-based differentiation protocol that yields functional and phenotypically accurate LECs (**Figure 1**), which can be used for tissue engineering, therapeutics, and drug screening purposes.

Results

Sodium acetate treatment results in expression of key lymphatic markers

We developed our differentiation protocol by modifying existing differentiation protocols for generic endothelial cells. Most existing growth factor-dependent differentiation protocols rely on the two-step process, where the hiPSC are first differentiated into mesodermal stage and then further differentiated into endothelial lineage.[35–37] We have tested modifications to protocols published by both Patsch and colleagues, and Harding and colleagues, and have found that the Harding protocol's 3 step process is better suited for LEC differentiation (**Supplementary Figure 1**).

To drive hiPSCs into their mesodermal lineage, we first culture hiPSCs as single cells suspension with 10 μM Y27632 for 2 days, followed by treatment with 50 ng/mL of VEGF-A, 25 ng/mL of BMP4, and 10 ng/mL of FGF2 for 2 days. After that, the differentiated cells were sorted for CD144 expression, and replated at 50,000-80,000 cells/cm^2 density, which should be optimized for each cell type (**Supplementary Figure 2**). Then the cells are treated with 50 ng/mL of VEGF-C and sodium acetate, a precursor molecule to acetyl-CoA, for 4 days (**Figure**

2A). Cells were cultured in STEMdiff APEL2 media for the first 4 days and then switched to microvascular endothelial growth medium (EGM-MV2) media for the last 4 days.

We optimized the concentration of sodium acetate added at the last stage and found that 50 mM concentration of sodium acetate (NaAc) in the final differentiation media results in optimal increase in lymphatic markers. We observed a 2.3-fold increase in podoplanin (*PDPN*) mRNA expression in cells treated with 20mM NaAc compared to 0 mM treatment, and we observed a 4.3-fold increase with 50 mM NaAc treatment (**Figure 2B**). We also observed a similar trend with flow cytometry data analyzing protein level expression of PDPN and LYVE-1, another key lymphatic marker (**Figure 2C-D**). We did not use concentrations higher than 50 mM as it resulted in high level of cell mortality. For all subsequent experiments, we subject the cells to 50 mM NaAc treatment along with 50 ng/mL VEGF-C for the final 4 days.

We observed a shift in CD31-expressing cell population to higher level of expression when treated with sodium acetate (**Figure 2E-F**). Our protocol resulted in between 80-90% of $CD31^+$ cells. When cells were treated with only VEGF-C and no sodium acetate, the protocol yielded less than 3% of $CD31^+/PDPN^+$ cells. However, with the addition of sodium acetate, the yield of the double-positive cells rose to approximately 40%. To ensure reproducibility of our protocol, we repeated this method with five different hiPSC cell lines derived from various cell types, as well as from male and female donors (**Supplementary Table 1**). We found similar increases in $CD31^+/PDPN_+$ cell yield with sodium acetate treatment (**Figure 2G, Supplementary Figure 3-7**).

We also tested for mRNA-level expression changes in *PDPN* and *VEGFR3* and found elevated levels of both LEC markers compared to native BECs, indicating sodium acetate treatment combined with VEGF-C results in expression of key lymphatic markers at the transcriptomic level. After 4 days of treatment, we observe a comparable level of *VEGFR3* expression compared to native LECs (**Figure 2H**). In fact, one cell line demonstrated over 3-

fold increase in expression of *VEGFR3* over native LECs. *PDPN*, which is a downstream marker from the VEGFR3-Prox1 feedback loop, also experienced over 5-fold increase in *PDPN* expression over BECs, at approximately 25% expression level of native LECs (**Figure 2I**). Taken together, these results indicate that sodium acetate treatment, when combined with VEGF-C treatment, can directly increase *VEGFR3* transcription which results in subsequent increases in the expression of key lymphatic markers.

Xeno-free differentiation yields improvement over co-culture method

Currently, the established method for differentiating stem cells into LECs relies on co-culture with a mouse stromal OP9 cell line. Kono and colleagues published a method to differentiate embryonic stem cells into LECs by co-culturing the VEGFR2^{+} cells in a sub-confluent culture of OP9 cells, then treated the cells with VEGF-C.[21] Similarly, others found that co-culturing hiPSC-derived early endothelial cells with OP9 cell line led to efficient differentiation into LECs.[20,38] As shown earlier, VEGF-C alone is not sufficient to induce LEC phenotypes in early endothelial cell line (**Figure 2G**), suggesting that OP9 plays a crucial and indispensable role in LEC differentiation. However, the reliance on a mouse cell line introduces potential complications in reproducibility and clinical relevance.

Therefore, we compared our differentiation protocol, which eliminates the need for OP9 cell line with the additional metabolite treatment along with VEGF-C, to the existing OP9 co-culture standards. We followed the protocol described Kono et al. for two hiPSC cell lines and compared the lymphatic marker expression with that of our dLECs. Our protocol yields drastically higher *VEGFR3* and *Prox1* expression for both hiPSC lines, indicating that our proposed pathway of inducing the VEGFR3-Prox1 positive feedback loop through sodium acetate treatment is more effective than the current OP9 method (**Figure 2J-K**). In addition,

our method also results in improvement of *PDPN* expression, which is downstream of our proposed feedback loop, indicating that our method not only activates the *Prox1* master regulator gene more effectively, but also results in a higher downstream lymphatic marker expression (**Figure 2L**). Taken together, these results indicate a significant improvement over the current standard of OP9 method, yielding higher lymphatic marker expression while also maintaining the benefits of a xeno-free differentiation method.

Differentiated LECs express Prox1, the master regulator of lymphatic identity

We hypothesized that the increase in VEGFR3 expression caused by the sodium acetate and VEGF-C treatment would subsequently affect *Prox1* expression, a master regulator of lymphatic identity. We performed our differentiation protocol with the removal of $CD144^-$ cells on day 4. Subsequently, we performed immunostaining on native LECs, native BECs, and our dLECs derived from three different iPSC cell lines (**Figure 3A**). We quantified the immunostaining images by selecting region of interest (ROI) based on DAPI stains through Cellpose, then calculating the average fluorescent intensity within each ROI. We observe comparable levels of ERG, a generic endothelial marker expressed in both BEC and LEC (**Figure 3B**). In comparison, we saw a comparable level of Prox1 expression in dLEC compared to LEC, while BEC saw negligible levels of Prox1 (**Figure 3C**).

We further show the expression of Prox1 using flow cytometry data. We observe that our dLECs express comparable levels of Prox1 compared to LEC, and significantly higher than BEC (**Figure 3D**). Interestingly, the i26 cell line seemed to have a statistically significant but significantly lower Prox1 expression compared to other dLECs and LEC, and more comparable to BECs. The remaining two cell lines that we tested demonstrated Prox1 levels of

approximately 50% of that of LECs. The i26 is the only cell line we tested that was PBMC-derived, indicating that fibroblast-derived hiPSC may be better suited for LEC differentiation. We further verified that the increase in Prox1 level is shown in RNA expression as well, although interestingly, the difference between dLEC and LEC in Prox1 RNA expression was more pronounced than that of protein level expression, indicating that there may be subtle differences in Prox1 transcription and translation in our dLECs (**Figure 3E**).

Differentiated LECs have similar transcriptomic profile to native LECs

In order to ascertain that our dLECs express LEC genes in addition to the identified marker genes, we performed an overall transcriptomic analysis on our cells compared to the native counterparts. We collected the RNA samples from the differentiated cells along with native LEC, BEC, and undifferentiated hiPSC and performed bulk RNA sequencing. We performed alignment analysis using STAR RNA-seq aligner and performed dimensionality reduction using principal component analysis on the resulting gene count matrix (**Supplementary Figure 8**). The resulting 2D plot shows our dLECs are highly similar to LECs and distinct from hiPSC (**Figure 4A**). Interestingly, the BECs and LECs have similar transcriptomic profile, given that the two cell types exhibit similar functionalities and physiology. We selected top 1% of genes with highest variability in expression level between LEC and hiPSC and plotted the Z-score for each sample type for each gene, and found that our dLECs are distinct from hiPSC and similar to LECs, while BECs have a distinct differential expression for several genes including (**Figure 4B**).

We also analyzed the expression levels of known lymphatic, endothelial, and pluripotency markers and found that our dLECs express comparable levels of all expected markers to that of LECs. Our dLECs express comparable levels of VE-cadherin, PECAM,

Foxc2, and ERG. The dLECs also express slightly lower, but still comparable, levels of PDPN, VWF, and Prox1, while expressing significantly higher levels of VEGFR3, most likely due to the direct effects of the sodium acetate treatment (**Figure 4C-L**). They also express no pluripotency markers such as Sox2, indicating that they are successfully differentiated into LECs.

Differentiated LECs secrete similar cytokines compared to native LECs

In addition to their role in forming lymphatic vessels, LECs have also been known to secrete cytokines that is responsible for the paracrine crosstalk between LECs and the surrounding cells. For example, LECs secrete reelin that promote cardiac organ maturation, and can also secrete CCL21 that promote the growth of glioblastoma stem cells.[11,39] Pathological LECs, such as LECs exposed to tumors, have also been shown to exhibit abnormal secretion of IL6 which promote primary tumor growth.[40] These findings suggest that the cytokine secretion is an important aspect of LEC functionality that influences the overall tissue development or tumor growth.

Therefore, we test for the cytokine production of our dLECs and compare them to native LECs. We collected the filtered supernatant from a confluent culture of various dLEC lines and given that adult and juvenile cell lines differ in cytokine production, we tested LECs from both juvenile and adult donors. We found that all dLECs secrete similar levels of reelin as adult LECs and slightly lower level compared to juvenile LEC (**Figure 5A**).[41] While several cells such as macrophages and fibroblasts have been known to secrete VEGF-C, LECs have not been found to secrete significant amounts of VEGF-C. As such, we found extremely low expression of VEGF-C secretion from all cell lines in the range of picograms per mL, as expected (**Figure 5B**).[42,43] In both VEGF-C and reelin secretion, dLECs expressed secretion levels similar to that

of adult LECs rather than juvenile LECs, which may be due to our iPSCs being derived from adult donors.

The proteome profiler assays demonstrated the presence of various lymphangiogenesis-related and anti-inflammatory proteins in both LECs and dLECs that are indicative of their potential therapeutic effect *in vivo* (**Figure 5, Supplementary Figure 9**). The prominent analytes, such as Serpin E1 (PAI-I), has been associated with improving lymphedema.[44] Pentraxin 3 (PTX3) has been found to be essential for LEC/vessel sprouting as well as the organization and function in lymphatic system.[45] Epidermal growth factor (EGF) has also been found to promote lymphatic vessel formation.[46] The presence of other lymphangiogenesis-related factors, such as angiopoietin-2 (Ang-2) and thrombospondin-1 (TSP-1), was also found in both LECs and dLECs thus further demonstrating its potential regenerative functionality *in vivo*.[47–50]

Differentiated LECs retain network formation capability of native LECs

To demonstrate that our dLECs retain the *in vitro* network formation capability, we compared the networks formed by native and differentiated LECs on two pro-angiogenic natural hydrogels, Matrigel and fibrin gels. Matrigel-based angiogenesis, first described in 1988, is a widely used standard to characterize the angiogenic capacity of endothelial cells, which is crucial for their application in tissue engineering.[51] Subsequent research has also identified other pro-angiogenic biomaterials that promote *in vitro* network formation and therefore has been used as a tool to measure the angiogenic potential of endothelial cells.[52,53] LECs have also been shown to form lymphatic networks similarly to their blood counterparts, and even maintain their ability to discriminate between blood and lymphatic lineage cells to form distinct networks when cultured together.[28]

We performed the network formation assays on growth factor reduced Matrigel and fibrin gel substrate, placed on a double-welled ibidi μ-slide. The cells, pre-stained with CellTracker Green CFMDA dye, were allowed to form networks for up to 24 hours, with imaging taking place every hour. Matrigel-seeded cells reached full network formation around 6 hours after seeding, and the fibrin-seeded cells reached its full network around 18 hours after seeding. The representative images of these networks at 6h and 18h are shown for both the LEC and dLEC, showing similar degree of vascularization (**Figure 6A, D**). We quantified the networks using AutoTube, a MATLAB-based software that performs skeletonization of the networks and performs quantification on the identified network.[54,55] We observed that the dLECs and LECs formed comparable networks, with similar branch point count and vessel width (**Figure 6B-C** and **E-F**). Interestingly, the dLECs formed slightly wider vessels on fibrin, but was comparable on the Matrigel. Overall, these results suggest that our dLECs developed the angiogenic potential that matches that of native LECs.

Differentiated LECs generate robust 3D lymphatic networks in synthetic hyaluronic acid hydrogels

Despite its widespread adoption, the traditional angiogenesis assay is limited by the 2D nature of the cell growth, which may not accurately capture the angiogenic environment *in vivo.* Therefore, we explored encapsulating the cell suspended in a hydrogel and analyzing the 3-dimensional (3D) network formation that better mimics *in vivo* angiogenesis. Specifically, LECs uniquely express LYVE-1, a lymphatic-specific homologue of CD44, which binds to hyaluronic acid to mediate lymphangiogenesis.[56,57] Our previous works have shown that hyaluronic acid hydrogels not only promote lymphatic vessel formation, but also is capable of modulating the lymphangiogenesis through stiffness modulation.[55,58]

For this study, we utilized hyaluronic acid hydrogels modified with norbornene (NorHA) which enabled UV-inducible thiol-norbornene crosslinking, along with matrix metalloproteinase (MMP)-sensitive crosslinker peptides to allow for matrix degradation and subsequently lymphatic network formation.[58,59] The cells were suspended into hyaluronic acid solution at a concentration of 4 and 8 million cells/mL, which were the optimal density range identified in our previous published work.[60] Following the UV-mediated crosslinking, the gels were cultured in media supplemented with 100 ng/mL of VEGF-C and FGF-2. We observed an extensive network formation by day 3 after crosslinking with dLEC-encapsulated gels, at which point the gels were fixed and stained for DAPI, F-actin, and VE-CAD (**Figure 6G**). As expected, the 8 million/mL gels formed more robust vascular network due to the higher cell density, while the 4 million/mL gels demonstrated a sparser network. We repeated the gel formation with native LEC and dLEC and stained for F-actin and found similar degree of network formation between dLEC and LEC (**Figure 6H-J**).

The 3D rendering of these vessels show that these vessels are indeed 3D and extend across the entire volume of the gel (**Figure 6K**). At 40x magnification, we see additionally that the dLECs are forming functional junctions based on the staining expression of VE-cadherin around the edges of the cell, along with the F-actin expression along the vessel formation (**Figure 6L**). We can additionally see that the vessels form a three-dimensional structure that closely mimic lumen and lymphatic button-like junctions, indicating that our dLECs are capable of forming highly accurate and robust lymphatic vasculature *in vitro* (**Figure 6M, Supplementary Movie S1**). These results suggest that our dLECs, similar to native LECs, can form robust lymphatic vasculature in an *in vitro* setting, which will allow them to be used in forming engineered tissues with functional lymphatic vessels.

Differentiated LECs promote lymphatic regeneration in mouse models

One of the potential applications of dLECs is in developing therapeutic options for secondary lymphedema. Currently, lymphedema treatments are limited to compression, anti-inflammatory drugs, and lifestyle changes.[61–63] Recent developments in lymphedema therapeutics include various pro-lymphangiogenic growth factors, indicating that promoting lymphangiogenesis may be a viable method to restore lymphatic functionality in secondary lymphedema.[64–69] Therefore, we explored the use of dLECs as a novel and fully autologous method to promote lymphatic regeneration in two relevant murine models: double-ligation tail lymphedema model and mammary fat pad model.

In the first murine model of double-ligation tail lymphedema model, we induced artificial lymphedema in mouse tails by ligating the two collecting lymphatic vessels and all surface lymphatics. This tail lymphedema model has been widely used and adapted for modeling secondary lymphedema by disrupting the lymphatic function across the tail, thereby causing swelling in the distal side of the tail similar to the symptoms of secondary lymphedema.[70,71] The disruption of the collecting vessels was shown to be sufficient to induce drastic lymphatic remodeling, with swelling taking up to 4 weeks to return to pre-injury levels.[72] In this study, we performed similar ligation of both collecting vessels and all superficial lymphatics and verified that the swelling reaches maximum level in about a week, which can be prevented through daily injection with non-steroidal anti-inflammatory drugs (NSAID; **Supplemental Figure 10**).

We injected dLECs suspended in Matrigel at concentration of 10 million cells/mL directly at the wound site and allowed the Matrigel to solidify for up to 15 minutes on a heating pad. The treatment group was compared with mice with no injection and mice with only Matrigel injected without cells. NSAID-treatment group was included as a positive control. We sacrificed the mice at day 7 to evaluate the efficacy of the dLECs in reducing swelling and restoring

lymphatic vessels (**Figure 7A**).[73] By day 5, a significant difference in swelling between the treatment and control groups was observed (**Figure 7B-D**). The mice that received Matrigel-dLECs injection experienced around 20% of the pre-injury level which was statistically non-significant compared to the NSAID-treatment group (**Figure 7E, Supplemental Figures 11-14**). In comparison, the mice with blank Matrigel injection and no injection experienced similar degree of swelling of around 40% increase from the pre-injury levels. Interestingly, the mice that received cell injection experience a sudden increase in swelling around day 7, which suggests initial immune reaction to xenogenic cells.

We sacrificed the mice at day 7 and collected the wound site sample from each mouse. We prepared histology samples sliced along the direction of the tail at the distal side of the wound and performed H&E staining. In all samples, we observe no major structures that indicate collecting lymphatic vessels, indicating that we have successfully disrupted the collecting vessels (**Figure 7F-I**). Since our dLECs mimic dermal LECs and do not contain necessary components of a collecting vessel such as lymphatic valve and lymphatic muscle cells, we do not expect the regeneration of lymphatic collecting vessels within this timeframe. We identified several lumen-like structures that are most likely superficial dermal lymphatics based on the presence of endothelial barrier along the edge of the lumen and lack of red blood cells to distinguish it from the blood vessels. Within these lymphatic-like lumens, we notice a higher deposition of elongated endothelial-like cells and macrophage-like multi-nucleated cells, indicating our dLECs are present within the lymphatic lumens (**Figure 7J-K**).

To further confirm the presence of our dLECs in the wound site, we collected histology samples distal to the wound site, where we surface lymphatic repair to begin. We performed immunohistochemistry staining for human CD31 and mouse PDPN to identify the interface between human dLECs and mouse LECs. Two representative tail samples, one from the group that received dLECs and one treated with blank Matrigel, are shown stained for mouse-PDPN

and human-CD31, with areas of interest emphasized (**Figure 7L, Supplemental Figure 17**). The positive stains are visible around the endothelium of the vessel lumen in both the human-CD31 and mouse-PDPN stains, indicating that the dLECs are contributing to the lymphatic repair process. We confirmed that the mice samples that received a blank Matrigel treatment exhibited few mouse-PDPN-positive vessels but lacked any human-CD31 expression in the vessels, along with the standard IgG negative control stains (**Supplemental Figures 15-16**). Lymphatic vessels were identified by the presence of PDPN-expressing endothelial cells surrounding the lumens of interest. In several of the identified lymphatic vessels, we observed chimeric vessels made of human and mouse cells, indicating that our dLECs are able to integrate into the host murine lymphatic vasculature.

To further investigate how human dLECs can integrate with the host murine lymphatic vessels, we used a second mouse model of murine mammary gland model, which has been previously used in the context of patient-derived tumor xenograft models of breast cancers.[74] Granular hydrogel constructs were fabricated using NorHA and cultured *in vitro* for two days to allow dLECs to begin to elongate and sprout, and then they were implanted into a pocket created in the #4 mammary gland of NOD/SCID mice.[58,75] To assess lymphatic integration, as well as to distinguish mouse vasculature from the implanted human LEC networks, two lectin dyes to label endothelial cells (ECs), one specific to mouse and the other one specific to human ECs, were injected into the extracellular space of the hindfoot for uptake to the lymphatic circulatory system before tissue harvest. The fluorescein-conjugated *Isolectin Griffonia simplicifolia* (*GS-IB$_4$* isolectin) stained mouse ECs, both blood and lymphatic, and the rhodamine-conjugated *Ulex Europaeus Agglutinin I (UEA-1* lectin*)* stained the human LECs[42,43]. While *UEA-1* lectin can stain both blood and lymphatic human ECs, the entirety of the rhodamine signal in these explants can be attributed to the implanted human LECs due to using a monoculture hydrogel system. In the granular gels, we observe lymphatic vessel-like

structures forming similar to the *in vitro* results we have published previously, which integrates with the mouse endothelial cells (**Figure 7M-N**). Taken together, these results suggest a potential therapeutic option for secondary lymphedema using patient-derived dLECs.

Discussion

Since the discovery of lymphatic-specific markers that made lymphatic vessel isolation possible, there has been an ever-increasing focus around the lymphatic system.[16,76] Despite its relative obscurity compared to its well-known blood circulatory counterpart, lymphatic vessels have been shown to play an indispensable role in critical tissue functions, such as fluid homeostasis and immune cell trafficking.[1–3] Therefore, lymphatic endothelial cells, which line the lymphatic vessels distinct from blood vessels, have been subject of focus for tissue engineering researchers with the intent to incorporate the lymphatic system into engineered tissue constructs. With the rise of stem cell engineering that aims to develop personalized therapies and drug screening platforms, the demand for hiPSC-derived LECs has grown, but to date, there is a lack of xeno-free and efficient differentiation method that captures both the lymphatic marker expression and LEC functionality.

We previously reported a direct differentiation of hiPSCs into LECs using transcription factor *ETV2* and *ETS2*.[77] While direct differentiation protocol can be used for disease modeling, the lentivirus used in the protocol may not be suitable for clinical applications. To complement this direct differentiation protocol, here we reported a step-wise differentiation using metabolic pathway by modifying the existing hiPSC-EC differentiation protocol, which utilizes a sequential differentiation from hiPSC to angioblasts, then to mature endothelial cells.[35] Based on the recent discoveries suggesting a population of LECs that are derived according to the centripetal theory from angioblasts, we utilized this differentiation protocol to reliably differentiate hiPSC

into LECs without needing to rely on transdifferentiation from blood ECs.[29] We have shown that with combination of VEGF-C and sodium acetate treatment, there is a sufficient upregulation of VEGFR3, which then upregulates Prox1 and subsequently further downstream lymphatic markers such as PDPN. We also showed that our cells retain the generic endothelial markers such as CD31, CD144, ERG, VWF, and others. When compared to the currently widely accepted differentiation protocol using the OP9 cell line, our differentiation protocol results in higher lymphatic marker expressions while also exclusively relying on xeno-free and fully defined components which improve the clinical applicability of these dLECs.

In addition, we have shown that our dLECs retain the full functionality of native LECs, including cytokine production, network formation, and lymphangiogenesis. In order to successfully integrate into engineered tissues, LECs are required to form lymphatic vessels which can then fulfill the native lymphatic functions such as fluid transport. Here, we showed that lymphangiogenic capacity of our dLECs match that of native LECs, in both traditional 2D angiogenesis assays and the novel 3D vessel formation assay that requires complex functions such as junction formation and matrix degradation. Furthermore, we show that the dLECs also have a similar cytokine secretion profile, which is crucial for surrounding organ development in *in vitro* organogenesis. We have shown that our dLECs are equally functional to native LECs, which demonstrates the potential for the dLECs to be incorporated into engineered tissues in order to model the lymphatic system.

We also demonstrated the potential therapeutic value of the dLECs through the mouse tail lymphedema model. Injection of the dLECs into mouse tail accelerated the lymphatic vessel repair, indicating that the dLECs are able to incorporate into the reconstructed lymphatic system. These results suggest that the dLECs, in addition to their value in creating *in vitro* lymphatic vessels, can also have direct therapeutic applications in lymphatic diseases such as lymphedema, where current treatment options are limited and primitive.[78] Taken together, we

conclude that our protocol yields robust, functional dLECs that match the native LECs in functionality and characteristics. Future works should explore the use of dLECs in applications such as organoid models and system-on-a-chip models to incorporate the indispensable functions of the lymphatic system into tissue engineering, as well as to evaluate the efficacy of these dLECs in clinically-relevant models of lymphedema.[79]

Methods

Human iPSC and LEC Culture

Human induced pluripotent stem cells derived from either skin or lung fibroblasts or peripheral blood mononuclear cells (WiCell, Stem Cell Technologies, ATCC) were expanded and used for experiments for up to 15 passages from initial purchase (**Supplementary Table 1**). Human iPSCs were seeded on tissue culture plastic surfaces coated with 0.083 mg/mL of Matrigel (Corning) in DMEM-F12 media (Gibco) and grown in mTeSR+ media (Stem Cell Technologies) at 37°C with 5% CO_2. 10 μM of Y-27632 Rho-kinase inhibitor was added to the cell culture media for the first day after seeding, then subsequently removed. Human LECs and BECs derived from the dermis of two adult donors (Promocell) were expanded and used between passages 5 and 8. The cells were cultured in MV2 media (Promocell) and similarly incubated at 37°C with 5% CO_2. LECs were characterized for the positive expression of CD31 and Prox1 throughout the experiments. All cell lines were routinely tested for mycoplasma contamination and were negative throughout this study.

Human iPSC Differentiation

Human iPSCs were passaged at between 60-80% confluency using Accutase and separated out into single cell suspension. The cells were passaged onto a new Matrigel-coated

plate at a concentration of between 30,000 and 50,000 cells per cm^2 of cell growth area. The exact seeding density was optimized for each cell line. Cells were treated with 10 μM of Y-27632 Rho-kinase inhibitor (Stem Cell Technologies) in mTeSR+ media (Stem Cell Technologies) for 1 day after passaging. Following this, cells were switched to APEL2 media (Stem Cell Technologies) containing 6 μM of CHIR99021 GSK inhibitor (Stem Cell Technologies) for 2 days without media change. On day 4, cells were switched to APEL2 media containing 50 ng/mL of VEGF-A (Stem Cell Technologies), 25 ng/mL of BMP-4 (R&D Biosystems), and 10 ng/mL of FGF-2 (R&D Biosystems) for 2 days, with media change each day.

At day 5, cells were passaged using TripLE Express media and re-seeded onto tissue culture plastic at density of 60,000 to 100,000 cells per cm^2. The cells were cultured in MV2 media (Promocell) containing 100 ng/mL of VEGF-C (R&D Biosystems) and 50 mM of sodium acetate (Thermo Fisher). Cells were cultured for 4 days with media change after 2 days. Following the differentiation, cells were passaged again for further experiments or used for RNA isolation.

Gene Expression

To analyze the gene expressions, we collected the RNA from dLECs on day 9 of differentiation, or 4 days after seeding for LEC and BEC. Each sample contained at least 3 biological replicates from cells cultured in distinct wells and analyzed with qRT-PCR. RNA was isolated using Qiagen Mini-prep kit (Qiagen), and quantified and diluted to the same concentration for all samples. The RNA was reverse transcribed using High-capacity cDNA reverse transcription kit (Thermo Fisher) using the recommended protocol from the manufacturer. We used TaqMan Gene expression assays (Thermo Fisher) following

manufacturer protocols and used *GAPDH* and *beta-actin* as endogenous controls to normalize relative gene expression levels using the $\Delta\Delta C_T$ method.

2D Network Formation Assay

The LECs and dLECs were first cultured to 70-80% confluency, then stained with 5μM CellTracker Green CFMDA (Thermo Fisher) for 30 minutes. The cells were passaged 24 hours later and seeded at a density of 30,000 cells per cm^2 onto the Ibidi 15 well μ-slide (Ibidi) containing either Matrigel or fibrin gel. The Matrigel was prepared by placing 10μL of growth factor reduced Matrigel (Corning) thawed out on ice to 4°C, then incubating at 37°C for 30 minutes. The fibrin gel was prepared by mixing 6μL of the fibrinogen solution with the 4μL of thrombin solution from the Angiogenesis Assay Kit (Millipore Sigma), and incubating at 37°C for 30 minutes. The cells were allowed to settle and attach for 1 hour after seeding, then imaged every hour for up to 24 hours.

Network Quantification

The fluorescent channel images from each well in the μ-slide were pre-processed by performing a rolling ball background subtraction with radius of 50 pixels on ImageJ. Then the resulting images were used as inputs to the AutoTube software and skeletonized. The skeletonized images were manually checked, and corrected as needed to remove holes in networks due to thresholding error. The resulting skeletonized images were analyzed using default settings, and the branch point and tube width data were collected for each replicate in each group.

RNA Sequencing Analysis

RNA samples were prepared using the Qiagen Mini-prep kit and further purified as needed to reach minimum A260/230 ratio of 1.8. The RNA samples were subsequently used for library prep using Illumina NextSeq P1 600 cycle at minimum read depth of 50 million per sample. The resulting sequencing readouts were aligned with the human genome using the STAR RNA-seq aligner, and the gene count matrix was generated.[80] The gene count matrix was normalized, then the top 1% of genes with the highest differential expression were selected. The resulting data matrix was used to perform the principal component analysis and generate a heat map, where the genes with the greatest differential expression between the control and the experimental groups were selected. The gene counts for several key genes of interest were extracted and subsequent statistical analyses were performed.

Cytokine ELISA

Supernatants were collected and filtered from confluent cultures of either LEC or dLEC. Media was changed 24 hours prior to supernatant collection to MV2 growth media (Promocell) that does not contain any additional growth factors. Supernatants were centrifuged at 300g for 5 minutes to pellet any cell debris. We quantified the relative total protein concentration using Bradford Protein Assay (Thermo Fisher) and diluted samples to the same concentration using PBS. The normalized supernatants were then quantified for cytokine content using ELISA kits for human VEGF-C and human reelin (Abcam). The absorbance values were quantified using Spark Microplate Reader (Tecan).

Proteome Profiler Arrays

Supernatants were collected and filtered from confluent cultures of either LEC or dLEC. Media was changed 24 hours prior to supernatant collection to MV2 growth media (Promocell) that does not contain any additional growth factors. Supernatants were centrifuged at 300g for

5 minutes to pellet any cell debris. The Proteome Profiler Human Angiogenesis Array Kit (R&D Systems) and Human XL Cytokine Array Kit (R&D Systems) were used to detect the expression of multiple proteins. Briefly, the supernatants were mixed with corresponding cocktails of biotinylated detection antibodies and incubated for 1 hour at room temperature. The mixtures were then incubated with array membranes containing specific capture antibodies to kit-specific target proteins overnight at 4°C on a plate shaker. The membranes were then washed to remove unbound material and incubated with streptavidin conjugated to horseradish-peroxidase (HRP) for 30 minutes at room temperature on a plate shaker. The membranes were then washed to remove excess streptavidin-HRP and were prepped with chemiluminescent detection reagents to be imaged using a ChemiDoc-It2 imager (UVP, Analytik Jena) and VisionWorks software (Analytik Jena). Quantification of the integrated pixel density of the duplicate spots was done using ImageJ and the MicroArray Profile plugin (OptiNav Software). Values from each membrane were normalized to an average pixel density value from respective reference spots.

Norbornene-modified Hyaluronic Acid Hydrogel Formation

Norbornene-modified hyaluronic acid polymers were synthesized using methods described in our previous publication with a 19% substitution of available functional groups with norbornene (19% D.S.).[59] The polymer was weighed out and mixed with PBS to the concentration of 2 wt%. Additionally, 0.5mg/mL of Irgacure 2959 (Sigma-Aldrich), 5 mM of RGD peptide (Genscript) and 2.6 mM of MMP-sensitive crosslinker (Genscript) were added to the mixture. The cells were passaged and resuspended in the polymer mixture. The polymer solution was placed into a mold of 50μL in volume and placed under 254 nm UV light at 10 mW/cm^2 intensity for 70 seconds to induce crosslinking, then placed into MV2 media (Promocell) containing 100 ng/mL of recombinant human VEGF-C (Bio-Techne), 100 ng/mL of

recombinant human bFGF (Stem Cell Technologies), and Antibiotic-Antimycotic (Thermo Fisher). Media was changed every day without disturbing the gel.

Immunofluorescence assay of hydrogels

Hydrogel samples were carefully placed on glass-bottom dish and fixed in 4% paraformaldehyde solution for 30 minutes at room temperature on the shaker. The gels were then blocked with 3% BSA solution for 1 hour at room temperature or overnight at 4°C on the shaker. Gels were stained with 300 nM DAPI solution for 30 minutes, then stained with 1:1000 dilution of the phalloidin-AF594 (Thermo Fisher) and VE Cadherin antibody conjugated with AF488 (Santa Cruz Biotechnology) on the shaker overnight. Between each stain the gels were washed 5 times with PBS, each with 5 minutes on the shaker. The gels were imaged on the Nikon AxR Confocal Microscope at either 10, 20, or 40x objective lenses. The resulting fluorescent images were used to generate 3D renderings using the IMARIS software.

Mouse tail lymphedema model

All animal studies were conducted in accordance with the relevant federal and local regulations and University of Notre Dame's IACUC protocol (protocol number 24-07-8678). C57BL/6J mice (The Jackson Laboratory) were anesthetized and the tail area sterilized using isopropanol and chlorohexidine wipes. The initial incision was made approximately 15mm away from the base of the tail around the entire circumference, while taking care to not sever the veins underneath the lymphatic collecting vessels. Any mice with noticeably heavy bleeding or necrotic tails, which indicate damage to the veins, were excluded from the study. Following the incision, the entire wound area was cauterized using a Bovie high temperature cauterizer (Aspen Surgical), then a topical antibiotic ointment was applied to the wound. Mice were treated with up to 0.05mL per 20 g weight of Ethiqa XR (MWI Animal Health), and the NSAID groups

were treated with up to 0.25mg per 20 g weight of meloxicam (MWI Animal Health). NSAID was administered every 24 hours and Ethiqa XR was administered as needed 72 hours after the initial surgery.

Mouse tail Matrigel and cell injection

For the Matrigel and Matrigel with cell treatment groups, we injected the respective materials 24 hours following the initial surgery. Growth factor reduced Matrigel (Corning) was thawed out on ice and mixed with dLECs at concentration of 10 million cells/mL. The cell-gel mixture or blank Matrigel were loaded into a syringe with 25-gauge needle and dispensed in the wounded area. The mice were placed on a heating pad under anesthesia for up to 15 minutes to allow for the gel to solidify. The wound area was then wrapped with bandage temporarily to prevent the gels from being disturbed.

Mouse tail imaging and sample collection

The mice were placed under anesthesia each day and photographed to track the tail swelling diameter. The mice tails were measured using a manual caliper and photographed, while any mice exhibiting necrosis were euthanized and excluded from the study. Following 7 days, the mice were sacrificed using CO_2 euthanasia chamber followed by cervical dislocation. The section of the mouse tail roughly 20mm long centered around the wound site were collected and placed in 4% formaldehyde solution overnight. The mice tail samples were cryo-sectioned and the H&E stains were prepared.

Mammary Fat Pad Model

Female NOD/SCID mice (3-4 weeks old) were used for the study as previously described in our previous studies. Briefly, granular hydrogel constructs were maintained in a sterile

environment and transferred to the animal facility for implantation into the mice. Under isoflurane anesthesia, an incision was made to access both the left and right #4 mammary gland. A pocket was then created with tweezers and the hydrogel construct was inserted into each pocket. Incisions were closed up with staples and mice were kept on a heating pad to recover from anesthesia, before being transferred back to their cage for daily monitoring (*n* = 4 per group). At the end of each experiment, mice were euthanatized using carbon dioxide chamber. We have complied with all relevant ethical regulation of animal use.

Two weeks post-implantation, two lectin dyes to label endothelial cells (ECs) of each species were injected into the extracellular space of the hindfoot for uptake to the lymphatic circulatory system before tissue harvest. The fluorescein-conjugated *Isolectin Griffonia simplicifolia* (*GS-IB*$_4$ isolectin) stained mouse ECs and the rhodamine-conjugated *Ulex Europaeus Agglutinin I (UEA-1* lectin*)* stained the human LECs. Hydrogels and the surrounding mammary gland tissue were then harvested. Tissues and hydrogels were arranged in cassettes and fixed with 4% PFA overnight, and then stored in sterile PBS. Due to low signal intensity and challenges with auto-fluorescence from the surrounding adipose tissue, some explants were stained a second time with the lectin dyes after fixation.

Tissues and hydrogels were then imaged as a whole-mount sample in a coverslip chamber-well with a Nikon AXR confocal microscope. The entire tissue area was scanned at 10x to determine the regions of vessel integration, and then z-stacks at 20x were taken to visualize the 3D structure and spatial arrangement of the vasculature. Regions of interest included where the mouse vasculature invaded the hydrogel region and where the human lymphatic vessels within the hydrogel continued to grow and connect with the host vasculature. Regions of fluorescent signal overlap were deemed areas of host-implant integration.

Statistical analysis

Statistical analysis was performed using GraphPad Prism software (GraphPad Software Inc., La Jolla, CA). All data where statistical analysis is reported were performed with minimum of three biological replicates. Statistical comparisons were made using Student's *t*-test to analyze the differences between the control and the experimental group. For the multiple comparisons, analysis of variance (ANOVA) was used followed by Tukey post hoc analysis. All results are expressed as mean ± SD, with individual data points shown alongside the mean. Significance levels are reported as *$p<0.05$, **$p<0.01$, ***$p<0.001$, ****$p<0.0001$.

Acknowledgements

We acknowledge support from the University of Notre Dame through "Advancing Our Vision" Initiative in Stem Cell Research, Harper Cancer Research Institute – American Cancer Society Institutional Research Grant (IRG-17-182-04), American Heart Association through Career Development Award (19-CDA-34630012 to D.H.-P.), National Science Foundation (2047903 and 2225601 to D.H-P.), National Institutes of Health (1R35-GM-143055 to D.H.-P.), National Science Foundation-Graduate Fellowships Program (NSF-GRFP to D.P.J.). We would like to thank Drs. Sarah Cole and Sarah Chapman from the Notre Dame Integrated Imaging Facility for performing confocal imaging and immunostaining analysis.

Conflict of interest statement: The authors have declared that no conflict of interest exists.

Author contributions: D.P.J. and D.H.-P. conceived the ideas, designed the experiments, interpreted the data, and wrote the manuscript. D.P.J., S.S., D.M., A.T., N.K.L., R.S.G., B.S. conducted the experiments and analyzed the data. J.B.D. helped and consulted with the animal studies. J.B.D. and D.H.-P. supervised the study. All authors have approved the manuscript.

Data and materials availability: Additional material and data which contributed to this study are present in the **Supplementary Information** and source data can be found in **Supplementary Data 1**.

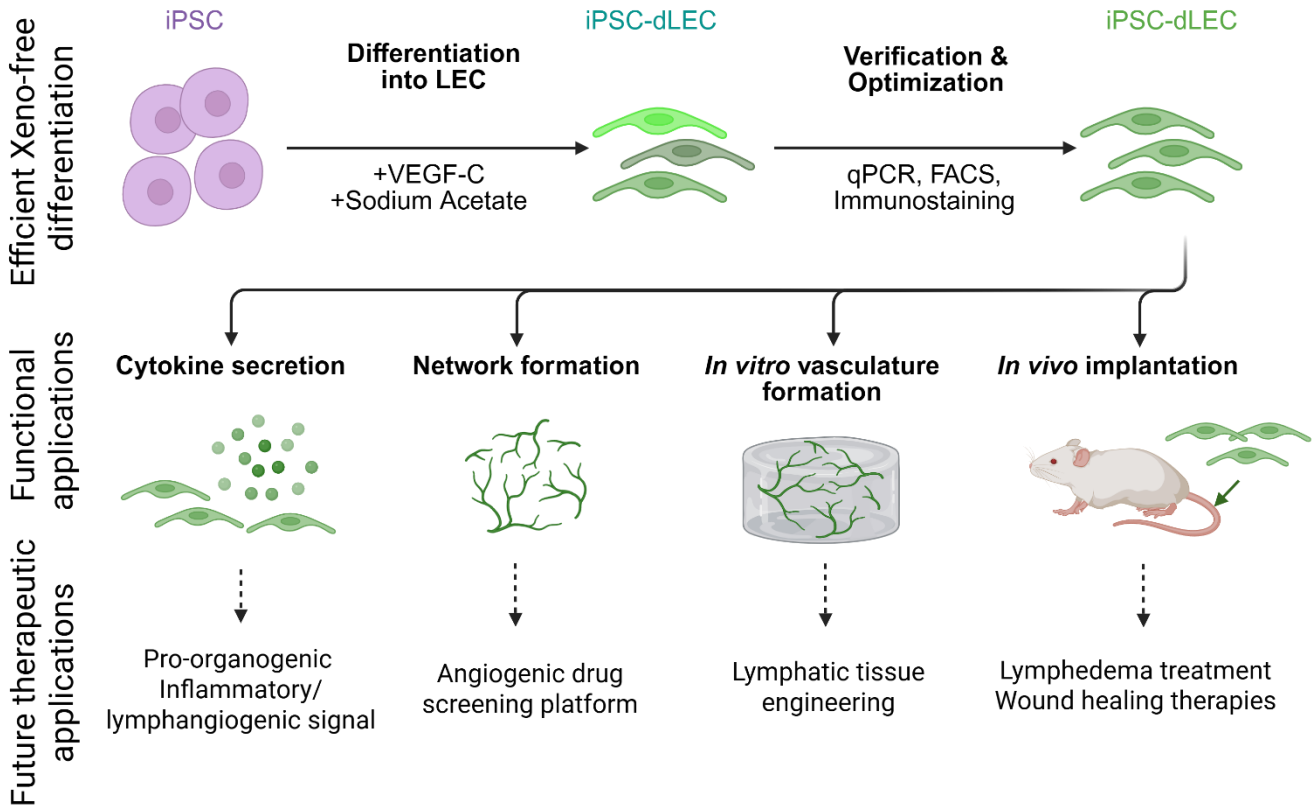

Figure 1. Overall schematic of the study. A xeno-free and stepwise differentiation protocol with VEGF-C and sodium acetate to differentiate five type of human induced pluripotent stem cells (hiPSCs) into lymphatic endothelial cells (LECs) with high efficiency and reproducibility. Differentiated LECs (dLECs) express key lymphatic markers as verified using bulk RNA-sequencing, qPCR, FACS, and immunostaining. These dLECs secrete important cytokines for lympangiocrine signaling, able to form robust 2D and 3D lymphatic networks, as well as demonstrate *in vivo* functionality and host integration in murine models.

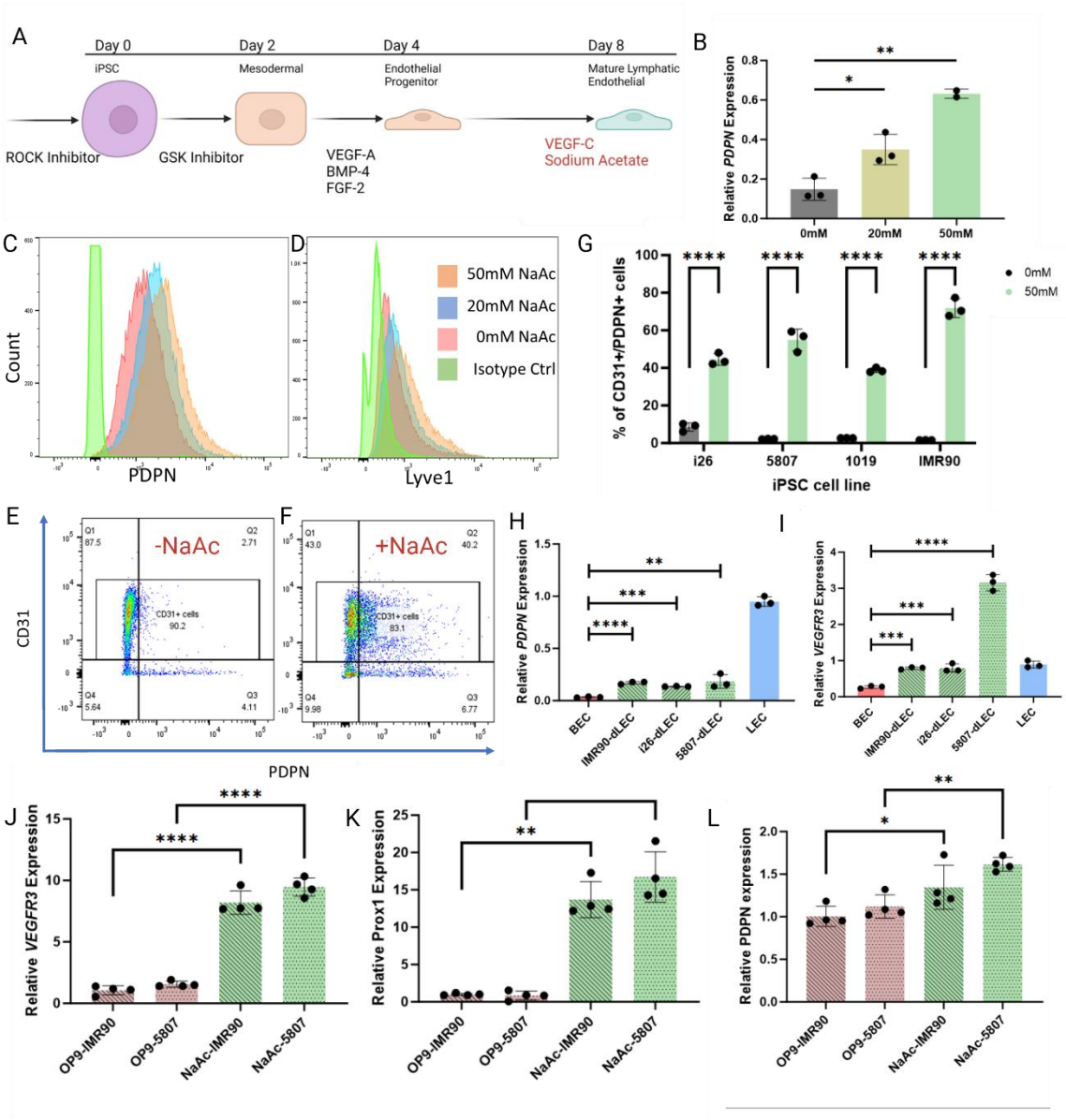

Figure 2. Expression of lymphatic markers with sodium acetate and VEGF-C treatment. (**A**) The differentiation schematic outlining our modifications to existing iPSC-EC differentiation protocol. (**B**) Relative podoplanin-mRNA expression for 0mM, 20mM, and 50mM NaAc treatment groups. The expression is shown as relative to GAPDH expression for each group. (**C-D**) Representative histogram showing shifts in PDPN and LYVE-1 expression as NaAc concentration increases. Isotype control is shown in light green and serves as a basis for

threshold for marker-expressing cells (**Supplementary Figure 2**). (**E-F**) FACS scatterplot for differentiated cells treated with and without NaAc showing an increase in PDPN+/CD31+ cell population. The boundaries were determined based on isotype controls for each marker. G) Percentage of $PDPN^{+}/CD31^{+}$ population resulting from our protocol with and without NaAc treatment without sorting step. For each iPSC cell line, we ran the differentiation protocol in triplicates. (**H**) VEGFR3 expression showing the increase in our differentiated cells compared to native BEC and LEC. (**I**) qPCR results showing an increase in PDPN expression in all three cell lines tested compared to BEC. (**J-L**) qPCR results showing a higher expression of three lymphatic markers in dLECs generated from our metabolite-based method when compared to the standard OP9-based method. *$p<0.05$, **$p<0.01$, ***$p<0.001$, ****$p<0.0001$. All statistical tests were performed with at least three replicate datapoints using Student's *t*-test.

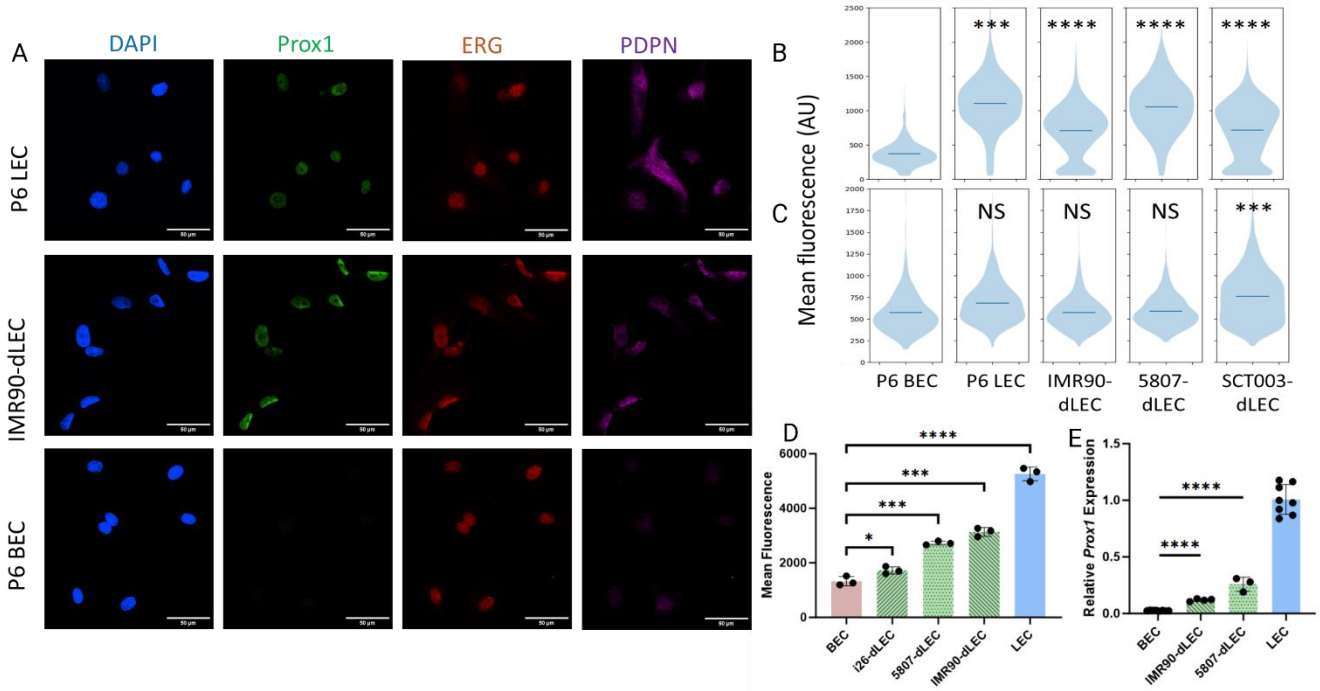

Figure 3. **Prox1 expression in the differentiated LECs.** (**A**) Immunostaining results comparing the expression of Prox1 and ERG between native LEC, BEC, and dLEC. The cells were fixed, permeabilized, then stained with DAPI, Prox1, ERG, and PDPN. Scale bar represents 50 μm. Representative images are shown. (**B-C**) Quantification of the immunostaining results. The nuclei of each cell were determined based on DAPI staining through Cellpose algorithm, then the average intensity for ERG and Prox1 channels were quantified for each cell. The overall population across all replicates are shown in the violin plot. All statistical significances are relative to the BEC condition. (**D**) Quantification for the FACS results based on the mean fluorescence intensity. Samples were double stained with ERG and Prox1, and ERG+ cells were selected and quantified for mean Prox1 signal. Each sample was run with 3 separately cultured and stained populations. (**E**) Real-time qPCR results showing an increase in Prox1 expression in all three cell lines tested compared to BEC. *p<0.05, **p<0.01, ***p<0.001, ****p<0.0001. All statistical tests were performed with at least three replicate datapoints using Student's t-test.

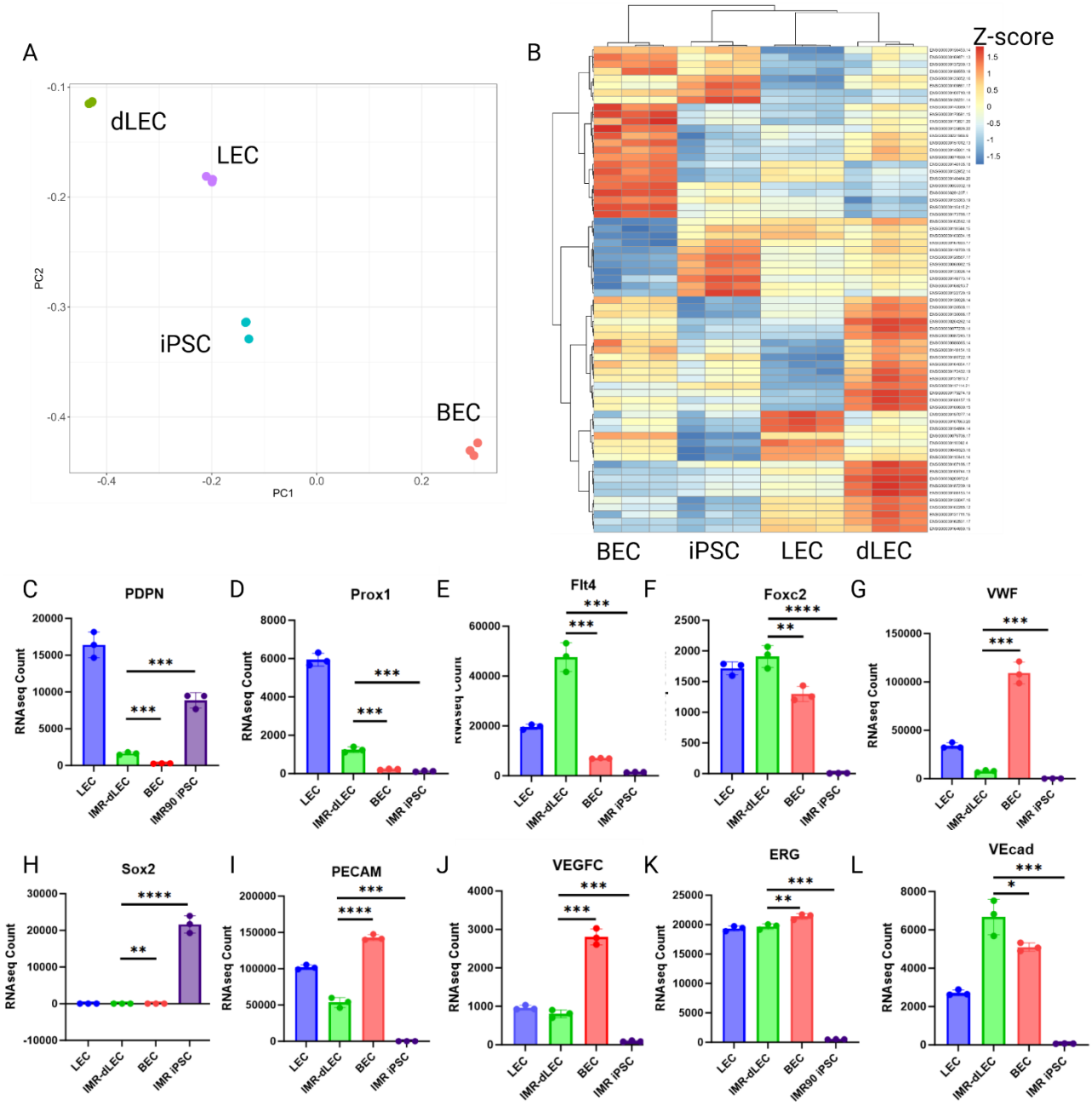

Figure 4. Bulk RNA sequencing results comparing iPSC, BEC, LEC, and dLEC. (**A**) Principal component analysis from the gene expression matrix result. Each point represents one biological replicate with RNA collected individually. The PCA was performed on the top 1% of the genes with the greatest standard deviation among the mean values for each cell type. (**B**) Heat map of the top 1% of the genes with the greatest variability, plotted with Ward.D2

clustering algorithm. (**C-L**) Select relevant endothelial, lymphatic, and pluripotent marker gene expression levels quantified from the gene expression matrix.

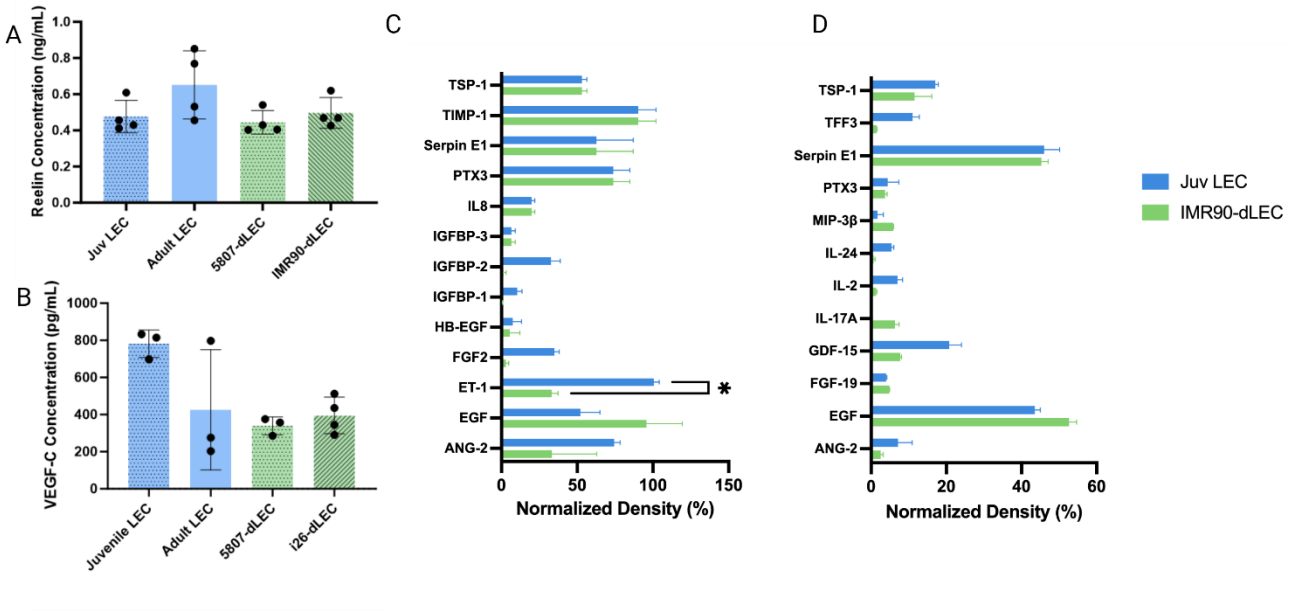

Figure 5. Cytokine and secretomic analysis. (**A**) Reelin ELISA analysis on the supernatants for juvenile, adult, and differentiated LECs. ANOVA result showed no significance. (**B**) VEGF-C ELISA analysis on the same supernatant samples. All samples showed secretion levels below 1 ng/mL. ANOVA results showed no significance. (**C-D**) Angiogenesis-related and inflammation-related cytokine array assay results. Only those with measurable level of signal detected via chemiluminescence is shown. Student t-test were performed for each cytokine type, with only ET-1 showing significance. Data represent mean $\pm$ SD, with n = 3-4 for ELISA and n = 2 for cytokine array.

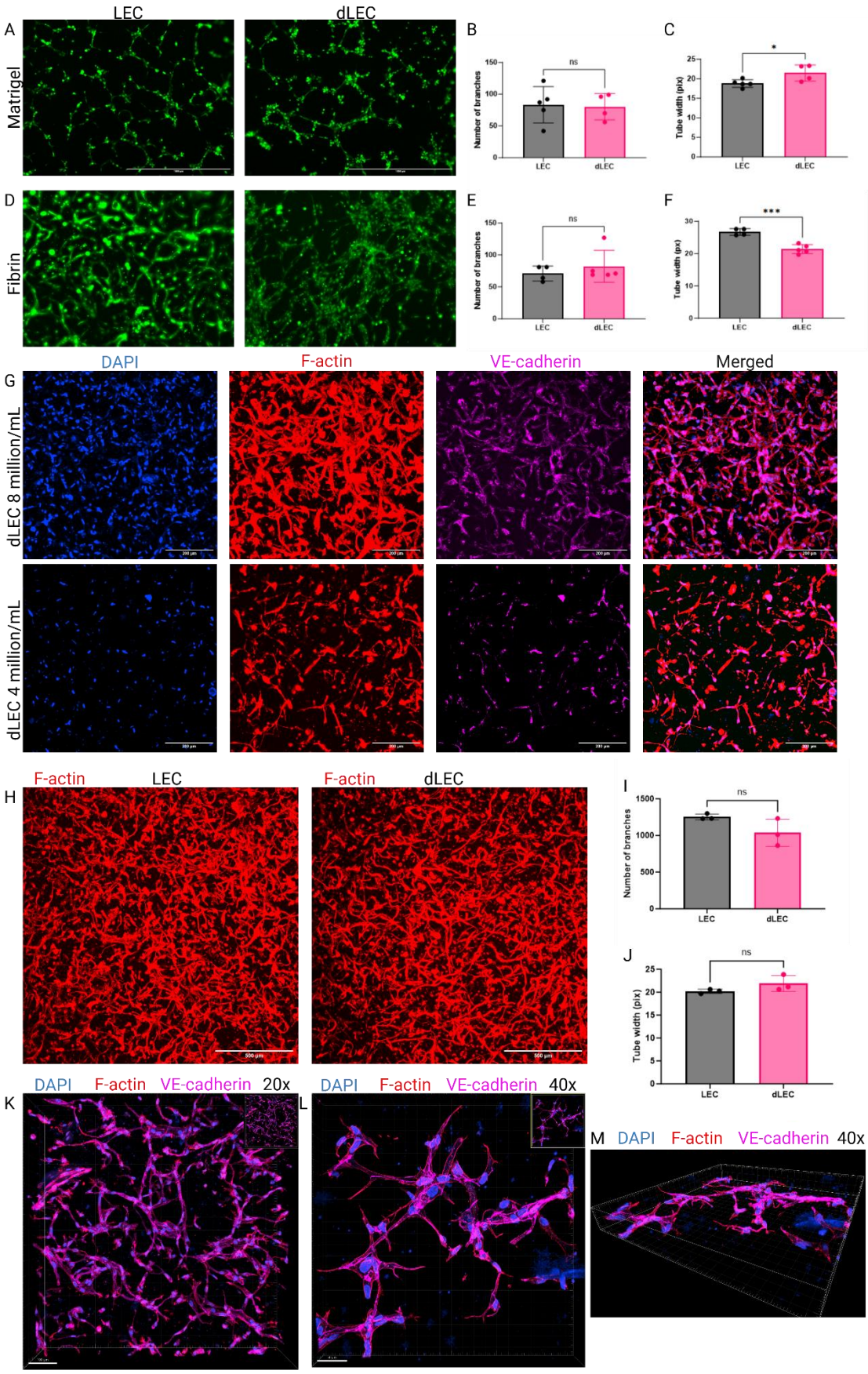
A
LEC
dLEC
Matrigel
B
C
Number of branches
Tube width (pix)
ns
*
LEC
dLEC
D
Fibrin
E
F
***
G
DAPI
F-actin
VE-cadherin
Merged
dLEC 8 million/mL
dLEC 4 million/mL
H
I
J
K
DAPI F-actin VE-cadherin 20x
L
DAPI F-actin VE-cadherin 40x
M
DAPI F-actin VE-cadherin 40x

752

Figure 6. 2D and 3D *in vitro* lymphatic vasculature formation. (**A,D**) Representative images of dLECs and native LECs forming networks in Matrigel and fibrin hydrogel surfaces. Selected images were taken 5 hours after initial seeding. Scale bar represents 1000 μm. (**B,C,E,F**) Quantification of the networks for number of branches and network width showing comparable levels between dLEC and LEC. G) Z-max projection images of dLEC vasculature in NorHA seeded at 4 and 8 million cells/mL staining for F-actin and VE-cadherin. Scale bar represents 200 μm. (**H**) Z-max projection of dLEC and LEC vasculature in NorHA stained for F-actin. Scale bar represents 500 μm. (**I-J**) Quantification of the max projection images for network branch count and tube width. (**K-M**) 3D rendering of the dLEC-NorHA vasculature showing VE-cadherin junctions and 3D structures. All statistical analysis performed using Student's *t*-test. *$p<0.05$, ***$p<0.001$.

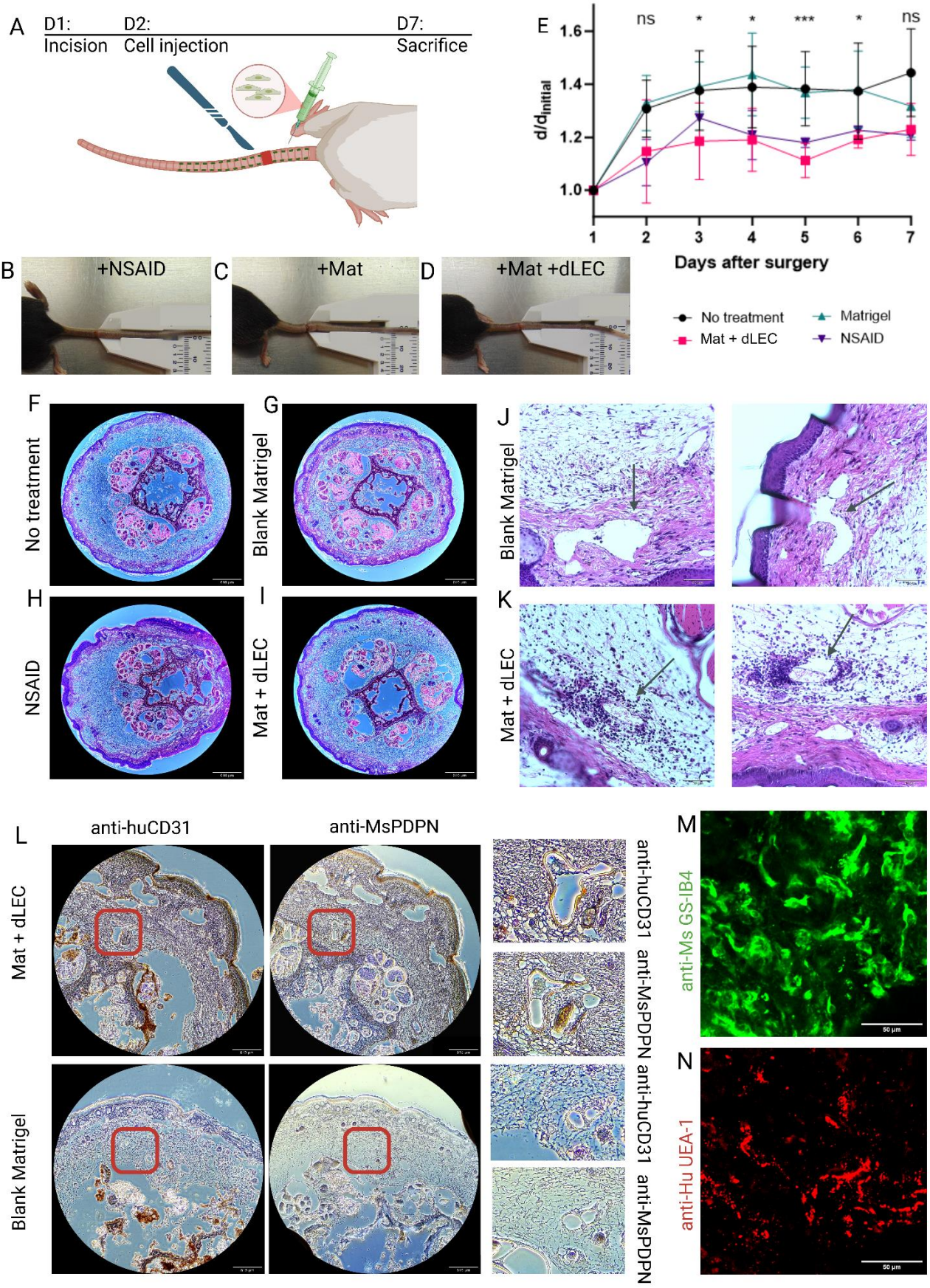
A
D1: Incision
D2: Cell injection
D7: Sacrifice
E
ns
*
*
***
*
ns
d/d_initial
1.6
1.4
1.2
1.0
1
2
3
4
5
6
7
Days after surgery
No treatment
Mat + dLEC
Matrigel
NSAID
B
+NSAID
C
+Mat
D
+Mat +dLEC
F
No treatment
G
Blank Matrigel
H
NSAID
I
Mat + dLEC
J
Blank Matrigel
K
Mat + dLEC
L
anti-huCD31
anti-MsPDPN
Mat + dLEC
Blank Matrigel
anti-huCD31
anti-MsPDPN
anti-huCD31
anti-MsPDPN
M
anti-Ms GS-IB4
N
anti-Hu UEA-1

765

Figure 7. *In vivo* functionality of differentiated LECs in murine models. (**A**) Schematic of the mouse tail lymphedema model. (**B-D**) Representative images of mice at day 5 following the surgery showing the differences in the degree of inflammation. (**E**) Changes in tail diameter for the 7 days following the surgery, normalized to the initial diameter. All statistical analysis is performed between the treatment dLEC group and blank Matrigel group. (**F-I**) H&E stains of the cross-sections of the wound site showing full disruption of the collecting lymphatics and most surface lymphatics. Scale bar is 860 μm. (**J-K**) Higher magnification images of the H&E staining focusing on the lymphatic lumens showing the presence of the dLECs in the wound site. Scale bar is 70 μm. (**L**) Immunohistochemistry slides of cross sections of the tail proximal to the wound site for blank Matrigel and Matrigel-dLEC treated group stained for mouse PDPN and human CD31, with areas of interest zoomed in. Positive stain is shown in brown. Scale bar is 860 μm. (**M-N**) Z-max projection images of the granular hydrogels stained with rhodamine-conjugated *Ulex Europaeus Agglutinin I* (*UEA-1 lectin*) for human endothelial cells and fluorescein-conjugated *Isolectin Griffonia simplicifolia* (*GS-IB 4* isolectin) for mouse endothelial cells. Scale bar represents 50 μm. All statistical analysis performed using Student's *t*-test. *$p<0.05$, ***$p<0.001$.

References

1. Charman WN, Stella VJ. Transport of lipophilic molecules by the intestinal lymphatic system. *Advanced Drug Delivery Reviews*. 1991;7(1):1-14. doi:10.1016/0169-409X(91)90046-F
2. Oliver G, Detmar M. The rediscovery of the lymphatic system: old and new insights into the development and biological function of the lymphatic vasculature. *Genes Dev*. 2002;16(7):773-783. doi:10.1101/gad.975002
3. Olszewski WL. The Lymphatic System in Body Homeostasis: Physiological Conditions. *Lymphatic Research and Biology*. 2003;1(1):11-24. doi:10.1089/15396850360495655
4. Sawdon M, Kirkman E. Capillary dynamics and the interstitial fluid–lymphatic system. *Anaesthesia & Intensive Care Medicine*. 2017;18(6):309-315. doi:10.1016/j.mpaic.2017.04.003
5. Swartz M. The physiology of the lymphatic system. *Advanced Drug Delivery Reviews*. 2001;50(1-2):3-20. doi:10.1016/S0169-409X(01)00150-8
6. Sleeman JP, Krishnan J, Kirkin V, Baumann P. Markers for the lymphatic endothelium: In search of the holy grail? *Microscopy Res & Technique*. 2001;55(2):61-69. doi:10.1002/jemt.1157
7. Sumpio BE, Timothy Riley J, Dardik A. Cells in focus: endothelial cell. *The International Journal of Biochemistry & Cell Biology*. 2002;34(12):1508-1512. doi:10.1016/S1357-2725(02)00075-4
8. Baldwin AL, Thurston G. Mechanics of Endothelial Cell Architecture and Vascular Permeability. *Crit Rev Biomed Eng*. 2001;29(2):247-278. doi:10.1615/CritRevBiomedEng.v29.i2.20
9. Sun X, Feinberg MW. Regulation of Endothelial Cell Metabolism: Just Go With the Flow. *ATVB*. 2015;35(1):13-15. doi:10.1161/ATVBAHA.114.304869
10. Tesfamariam B, Cohen RA. Inhibition of adrenergic vasoconstriction by endothelial cell shear stress. *Circ Res*. 1988;63(4):720-725. doi:10.1161/01.RES.63.4.720
11. Mantovani A, Bussolino F, Dejana E. Cytokine regulation of endothelial cell function. *FASEB j*. 1992;6(8):2591-2599. doi:10.1096/fasebj.6.8.1592209
12. Ji RC. Lymphatic Endothelial Cells, Lymphedematous Lymphangiogenesis, and Molecular Control of Edema Formation. *Lymphatic Research and Biology*. 2008;6(3-4):123-137. doi:10.1089/lrb.2008.1005
13. Ly C, Kataru R, Mehrara B. Inflammatory Manifestations of Lymphedema. *IJMS*. 2017;18(1):171. doi:10.3390/ijms18010171
14. Liu X, De la Cruz E, Gu X, et al. Lymphoangiocrine signals promote cardiac growth and repair. *Nature*. 2020;588(7839):705-711. doi:10.1038/s41586-020-2998-x
15. Alexander A, Herz J, Calvier L. Reelin through the years: From brain development to inflammation. *Cell Reports*. 2023;42(6):112669. doi:10.1016/j.celrep.2023.112669
16. Alderfer L, Wei A, Hanjaya-Putra D. Lymphatic Tissue Engineering and Regeneration. *J Biol Eng*. 2018;12(1):32. doi:10.1186/s13036-018-0122-7
17. Nagahara AI, Homma J, Ryu B, et al. Networked lymphatic endothelial cells in a transplanted cell sheet contribute to form functional lymphatic vessels. *Sci Rep*. 2022;12(1):21698. doi:10.1038/s41598-022-26041-0
18. Niklason LE, Koh J, Solan A. Tissue Engineering of the Lymphatic System. *Annals of the New York Academy of Sciences*. 2002;979(1):27-34. doi:10.1111/j.1749-6632.2002.tb04864.x

19. Schaupper M, Jeltsch M, Rohringer S, Redl H, Holnthoner W. Lymphatic Vessels in Regenerative Medicine and Tissue Engineering. *Tissue Engineering Part B: Reviews*. 2016;22(5):395-407. doi:10.1089/ten.teb.2016.0034
20. Lee SJ, Park C, Lee JY, et al. Generation of pure lymphatic endothelial cells from human pluripotent stem cells and their therapeutic effects on wound repair. *Sci Rep*. 2015;5(1):11019. doi:10.1038/srep11019
21. Kono T, Kubo H, Shimazu C, et al. Differentiation of Lymphatic Endothelial Cells From Embryonic Stem Cells on OP9 Stromal Cells. *ATVB*. 2006;26(9):2070-2076. doi:10.1161/01.ATV.0000225770.57219.b0
22. Jiao YC, Wang YX, Liu WZ, et al. Advances in the differentiation of pluripotent stem cells into vascular cells. *World J Stem Cells*. 2024;16(2):137-150. doi:10.4252/wjsc.v16.i2.137
23. Ribatti D, Crivellato E. The embryonic origins of lymphatic vessels: an historical review. *Br J Haematol*. 2010;149(5):669-674. doi:10.1111/j.1365-2141.2009.08053.x
24. Sasaki K, Yokobayashi S, Nakamura T, et al. Robust In Vitro Induction of Human Germ Cell Fate from Pluripotent Stem Cells. *Cell Stem Cell*. 2015;17(2):178-194. doi:10.1016/j.stem.2015.06.014
25. Matsuda M, Yamanaka Y, Uemura M, et al. Recapitulating the human segmentation clock with pluripotent stem cells. *Nature*. 2020;580(7801):124-129. doi:10.1038/s41586-020-2144-9
26. Esfahani SN, Zheng Y, Arabpour A, et al. Derivation of human primordial germ cell-like cells in an embryonic-like culture. *Nat Commun*. 2024;15(1):167. doi:10.1038/s41467-023-43871-2
27. Cooley LS, Handsley MM, Zhou Z, et al. Reversible transdifferentiation of blood vascular endothelial cells to a lymphatic-like phenotype in vitro. *Journal of Cell Science*. 2010;123(21):3808-3816. doi:10.1242/jcs.064279
28. Jeong DP, Hall E, Neu E, Hanjaya-Putra D. Podoplanin is Responsible for the Distinct Blood and Lymphatic Capillaries. *Cel Mol Bioeng*. 2022;15(5):467-478. doi:10.1007/s12195-022-00730-2
29. Lupu IE, Grainger DE, Kirschnick N, et al. Direct specification of lymphatic endothelium from mesenchymal progenitors. *Nat Cardiovasc Res*. 2025;4(1):45-63. doi:10.1038/s44161-024-00570-5
30. Jang S, Collin De l'Hortet A, Soto-Gutierrez A. Induced Pluripotent Stem Cell–Derived Endothelial Cells. *The American Journal of Pathology*. 2019;189(3):502-512. doi:10.1016/j.ajpath.2018.12.004
31. D'Souza SS, Kumar A, Slukvin II. Functional Heterogeneity of Endothelial Cells Derived from Human Pluripotent Stem Cells. *Stem Cells and Development*. 2018;27(8):524-533. doi:10.1089/scd.2017.0238
32. Morfoisse F, Renaud E, Hantelys F, Prats AC, Garmy-Susini B. Role of hypoxia and vascular endothelial growth factors in lymphangiogenesis. *Molecular & Cellular Oncology*. 2015;2(4):e1024821. doi:10.1080/23723556.2015.1024821
33. Wong BW, Wang X, Zecchin A, et al. The role of fatty acid β-oxidation in lymphangiogenesis. *Nature*. 2017;542(7639):49-54. doi:10.1038/nature21028
34. Zecchin A, Wong BW, Tembuyser B, et al. Live imaging reveals a conserved role of fatty acid β-oxidation in early lymphatic development in zebrafish. *Biochemical and Biophysical Research Communications*. 2018;503(1):26-31. doi:10.1016/j.bbrc.2018.04.233
35. Harding A, Cortez-Toledo E, Magner NL, et al. Highly Efficient Differentiation of Endothelial Cells from Pluripotent Stem Cells Requires the MAPK and the PI3K Pathways. *Stem Cells*. 2017;35(4):909-919. doi:10.1002/stem.2577

36. Patsch C, Challet-Meylan L, Thoma EC, et al. Generation of vascular endothelial and smooth muscle cells from human pluripotent stem cells. *Nat Cell Biol*. 2015;17(8):994-1003. doi:10.1038/ncb3205
37. Sahara M, Hansson EM, Wernet O, Lui KO, Später D, Chien KR. Manipulation of a VEGF-Notch signaling circuit drives formation of functional vascular endothelial progenitors from human pluripotent stem cells. *Cell Res*. 2014;24(7):820-841. doi:10.1038/cr.2014.59
38. Vittet D, Merdzhanova G, Prandini M, Feige J, Bailly S. TGFβ1 inhibits lymphatic endothelial cell differentiation from mouse embryonic stem cells. *Journal Cellular Physiology*. 2012;227(11):3593-3602. doi:10.1002/jcp.24063
39. Zhao L, Qiu Z, Yang Z, et al. Lymphatic endothelial-like cells promote glioblastoma stem cell growth through cytokine-driven cholesterol metabolism. *Nat Cancer*. 2024;5(1):147-166. doi:10.1038/s43018-023-00658-0
40. Van De Velde M, Ebroin M, Durré T, et al. Tumor exposed-lymphatic endothelial cells promote primary tumor growth via IL6. *Cancer Letters*. 2021;497:154-164. doi:10.1016/j.canlet.2020.10.020
41. Lilic D, Cant AJ, Abinun M, Calvert JE, Spickett GP. Cytokine Production Differs in Children and Adults. *Pediatr Res*. 1997;42(2):237-240. doi:10.1203/00006450-199708000-00018
42. Cursiefen C, Chen L, Borges LP, et al. VEGF-A stimulates lymphangiogenesis and hemangiogenesis in inflammatory neovascularization via macrophage recruitment. *J Clin Invest*. 2004;113(7):1040-1050. doi:10.1172/JCI20465
43. Wang G, Muhl L, Padberg Y, et al. Specific fibroblast subpopulations and neuronal structures provide local sources of Vegfc-processing components during zebrafish lymphangiogenesis. *Nat Commun*. 2020;11(1):2724. doi:10.1038/s41467-020-16552-7
44. Saik OV, Nimaev VV, Usmonov DB, et al. Prioritization of genes involved in endothelial cell apoptosis by their implication in lymphedema using an analysis of associative gene networks with ANDSystem. *BMC Med Genomics*. 2019;12(S2):47. doi:10.1186/s12920-019-0492-9
45. Doni A, Sironi M, Del Prete A, et al. PTX3 is expressed in terminal lymphatics and shapes their organization and function. *Front Immunol*. 2024;15:1426869. doi:10.3389/fimmu.2024.1426869
46. Marino D, Angehrn Y, Klein S, et al. Activation of the epidermal growth factor receptor promotes lymphangiogenesis in the skin. *Journal of Dermatological Science*. 2013;71(3):184-194. doi:10.1016/j.jdermsci.2013.04.024
47. Gale NW, Thurston G, Hackett SF, et al. Angiopoietin-2 Is Required for Postnatal Angiogenesis and Lymphatic Patterning, and Only the Latter Role Is Rescued by Angiopoietin-1. *Developmental Cell*. 2002;3(3):411-423. doi:10.1016/S1534-5807(02)00217-4
48. Norrmén C, Ivanov KI, Cheng J, et al. FOXC2 controls formation and maturation of lymphatic collecting vessels through cooperation with NFATc1. *Journal of Cell Biology*. 2009;185(3):439-457. doi:10.1083/jcb.200901104
49. Singla B, Aithbathula RV, Pervaiz N, et al. CD47 Activation by Thrombospondin-1 in Lymphatic Endothelial Cells Suppresses Lymphangiogenesis and Promotes Atherosclerosis. *ATVB*. 2023;43(7):1234-1250. doi:10.1161/ATVBAHA.122.318904
50. Hawighorst T, Oura H, Streit M, et al. Thrombospondin-1 selectively inhibits early-stage carcinogenesis and angiogenesis but not tumor lymphangiogenesis and lymphatic metastasis in transgenic mice. *Oncogene*. 2002;21(52):7945-7956. doi:10.1038/sj.onc.1205956

51. Kubota Y, Kleinman HK, Martin GR, Lawley TJ. Role of laminin and basement membrane in the morphological differentiation of human endothelial cells into capillary-like structures. *The Journal of cell biology*. 1988;107(4):1589-1598. doi:10.1083/jcb.107.4.1589
52. Hooks JST, Bernard FC, Cruz-Acuña R, et al. Synthetic hydrogels engineered to promote collecting lymphatic vessel sprouting. *Biomaterials*. 2022;284:121483. doi:10.1016/j.biomaterials.2022.121483
53. Hanjaya-Putra D, Bose V, Shen YI, et al. Controlled activation of morphogenesis to generate a functional human microvasculature in a synthetic matrix. *Blood*. 2011;118(3):804 LP - 815.
54. Montoya-Zegarra JA, Russo E, Runge P, et al. AutoTube: a novel software for the automated morphometric analysis of vascular networks in tissues. *Angiogenesis*. 2019;22(2):223-236. doi:10.1007/s10456-018-9652-3
55. Bui L, Edwards S, Hall E, et al. Engineering bioactive nanoparticles to rejuvenate vascular progenitor cells. *Communications Biology*. 2022;5(1):635. doi:10.1038/s42003-022-03578-4
56. Banerji S, Ni J, Wang SX, et al. LYVE-1, a New Homologue of the CD44 Glycoprotein, Is a Lymph-specific Receptor for Hyaluronan. *The Journal of Cell Biology*. 1999;144(4):789-801. doi:10.1083/jcb.144.4.789
57. Wu M, Du Y, Liu Y, et al. Low Molecular Weight Hyaluronan Induces Lymphangiogenesis through LYVE-1-Mediated Signaling Pathways. Addison CL, ed. *PLoS ONE*. 2014;9(3):e92857. doi:10.1371/journal.pone.0092857
58. Alderfer L, Saha S, Fan F, Wu J, Littlepage LE, Hanjaya-Putra D. Multi-parameter tunable synthetic matrix for engineering lymphatic vessels. *Commun Biol*. 2024;7(1):1-13. doi:10.1038/s42003-024-06935-7
59. Fan F, Su B, Kolodychak A, et al. Hyaluronic Acid Hydrogels with Phototunable Supramolecular Cross-Linking for Spatially Controlled Lymphatic Tube Formation. *ACS Appl Mater Interfaces*. 2023;15(50):58181-58195. doi:10.1021/acsami.3c12514
60. Alderfer L, Russo E, Archilla A, Coe B, Hanjaya-Putra D. Matrix stiffness primes lymphatic tube formation directed by vascular endothelial growth factor-C. *FASEB j*. 2021;35(5). doi:10.1096/fj.202002426RR
61. Keith L, Rowsemitt C, Richards LG. Lifestyle Modification Group for Lymphedema and Obesity Results in Significant Health Outcomes. *American Journal of Lifestyle Medicine*. 2020;14(4):420-428. doi:10.1177/1559827617742108
62. Uzkeser H, Karatay S, Erdemci B, Koc M, Senel K. Efficacy of manual lymphatic drainage and intermittent pneumatic compression pump use in the treatment of lymphedema after mastectomy: a randomized controlled trial. *Breast Cancer*. 2015;22(3):300-307. doi:10.1007/s12282-013-0481-3
63. Barufi S, Pereira De Godoy HJ, Pereira De Godoy JM, Guerreiro Godoy MDF. Exercising and Compression Mechanism in the Treatment of Lymphedema. *Cureus*. Published online 2 July 2021. doi:10.7759/cureus.16121
64. Karkkainen MJ, Saaristo A, Jussila L, et al. A model for gene therapy of human hereditary lymphedema. *Proc Natl Acad Sci USA*. 2001;98(22):12677-12682. doi:10.1073/pnas.221449198
65. Szuba A, Skobe M, Karkkainen MJ, et al. Therapeutic lymphangiogenesis with human recombinant VEGF-C. *FASEB j*. 2002;16(14):1985-1987. doi:10.1096/fj.02-0401fje
66. Jin DP, An A, Liu J, Nakamura K, Rockson SG. Therapeutic Responses to Exogenous VEGF-C Administration in Experimental Lymphedema: Immunohistochemical and

Molecular Characterization. *Lymphatic Research and Biology*. 2009;7(1):47-57. doi:10.1089/lrb.2009.0002

67. Hadamitzky C, Zaitseva TS, Bazalova-Carter M, et al. Aligned nanofibrillar collagen scaffolds – Guiding lymphangiogenesis for treatment of acquired lymphedema. *Biomaterials*. 2016;102:259-267. doi:10.1016/j.biomaterials.2016.05.040
68. Kajiya K, Hirakawa S, Ma B, Drinnenberg I, Detmar M. Hepatocyte growth factor promotes lymphatic vessel formation and function. *EMBO J*. 2005;24(16):2885-2895. doi:10.1038/sj.emboj.7600763
69. Michalaki E, Rudd JM, Liebman L, et al. Lentiviral overexpression of VEGFC in transplanted MSCs leads to resolution of swelling in a mouse tail lymphedema model. *Microcirculation*. 2023;30(2-3):e12792. doi:10.1111/micc.12792
70. Clavin NW, Avraham T, Fernandez J, et al. TGF-β_1 is a negative regulator of lymphatic regeneration during wound repair. *American Journal of Physiology-Heart and Circulatory Physiology*. 2008;295(5):H2113-H2127. doi:10.1152/ajpheart.00879.2008
71. Rutkowski JM, Boardman KC, Swartz MA. Characterization of lymphangiogenesis in a model of adult skin regeneration. *American Journal of Physiology-Heart and Circulatory Physiology*. 2006;291(3):H1402-H1410. doi:10.1152/ajpheart.00038.2006
72. Weiler MJ, Cribb MT, Nepiyushchikh Z, Nelson TS, Dixon JB. A novel mouse tail lymphedema model for observing lymphatic pump failure during lymphedema development. *Sci Rep*. 2019;9(1):10405. doi:10.1038/s41598-019-46797-2
73. Farrokhi A, Rahavi M, Jo S, et al. Inflammatory Immune Responses Trigger Rejection of Allogeneic Fibroblasts Transplanted into Mouse Skin. *Cell Transplant*. 2022;31:09636897221113803. doi:10.1177/09636897221113803
74. Suarez CD, Littlepage LE. Patient-Derived Tumor Xenograft Models of Breast Cancer BT - Breast Cancer: Methods and Protocols. In: Cao J, ed. Springer New York; 2016:211-223. doi:10.1007/978-1-4939-3444-7_19
75. Montes D, Saha S, Taglione A, et al. Tuning the Morphological Properties of Granular Hydrogels to Control Lymphatic Capillary Formation. *Adv Materials Inter*. Published online 24 April 2025:2401037. doi:10.1002/admi.202401037
76. Alderfer L, Hall E, Hanjaya-Putra D. Harnessing biomaterials for lymphatic system modulation. *Acta Biomaterialia*. 2021;133:34-45. doi:10.1016/j.actbio.2021.06.006
77. Saha S, Graham F, Knopp J, Patzke C, Hanjaya-Putra D. Robust Differentiation of Human Pluripotent Stem Cells into Lymphatic Endothelial Cells Using Transcription Factors. *Cells Tissues Organs*. Published online 28 August 2024:1-11. doi:10.1159/000539699
78. Warren AG, Brorson H, Borud LJ, Slavin SA. Lymphedema: A Comprehensive Review. *Annals of Plastic Surgery*. 2007;59(4):464-472. doi:10.1097/01.sap.0000257149.42922.7e
79. Nelson TS, Nepiyushchikh Z, Hooks JST, et al. Lymphatic remodelling in response to lymphatic injury in the hind limbs of sheep. *Nature Biomedical Engineering*. 2020;4(6):649-661. doi:10.1038/s41551-019-0493-1
80. Dobin A, Davis CA, Schlesinger F, et al. STAR: ultrafast universal RNA-seq aligner. *Bioinformatics*. 2013;29(1):15-21. doi:10.1093/bioinformatics/bts635